Acta Mech 220, 275–287 (2011)
DOI 10.1007/s00707-011-0482-2

Pu Zhang · Yiming Fu

Torsional buckling of elastic cylinders with hard coatings

Received: 11 March 2010 / Published online: 1 April 2011

Abstract The torsional buckling characteristic of an elastic cylinder with a hard surface coating layer is addressed in this paper. Deformations of the core and surface layer are obtained analytically through the Navier's equation and thin shell model, respectively. Both infinitely and finitely long cylinders are studied and the effects of the surface layer's stiffness, thickness, residual stresses, as well as the cylinder lengths on the critical torsional angle and buckling morphologies, are discussed. It is found that either the surface rippling or global buckling mode may occur when there exist residual stresses within the surface layer. The critical torsional angle increases when the surface layer becomes stiffer and thinner. In addition, higher-order rippling modes frequently occur for a finite-length cylinder with stiffer and thinner surface layer.

1 Introduction

Elastic cylinders with hard surface coating layers are quite commonly seen in both nature and engineering. For instance, porcupine quills and many plant stems all have stiff outer shells supported by soft cellular cores [1]. These natural structures usually have high buckling resistance loads but low weight, which enlightened the biomimick design of engineering cylindrical shells [2] with better mechanical properties. Moreover, it was reported that hard surface coatings, which are deposited or created by surface treatment on plastics and polymers [3], can improve the wear resistance [4] or adhesion properties [5] of them. This kind of core-shell structures can also exist in electro spun fibers, which are formed by either solidification of two fluids [6] or an evaporation process [7]. In addition, the surface effect of nanowires is usually modeled as a thin surface layer [8], either harder or softer than the core [9].

Static stability analyses are always drawn much attention to by researchers and structural designers, which include the torsional buckling problems induced by applied torques. After the pioneering study on torsional buckling properties of shells by Donnell [10], Yamaki [11] reported approximate solutions that were in reasonable agreement with experimental results, and Kim et al. [12] presented three-dimensional solutions to thick orthotropic cases. Thereafter, Zhang and Han [13] obtained more exact solutions, which account for the initial imperfection as well as boundary layer effects. It should also be mentioned that cylindrical shells in torsion would encounter a local buckling process prior to the system failure, which is quite different from the perfect axially compressed cases [14]. Other torsional buckling problems are also studied by researchers for composite [15] or functionally graded [16] cylindrical shells, which will not be introduced in detail here. Aside from the cylindrical shells, torsional characteristics of elastic rods are quite significant and also amazing, which

P. Zhang (✉) · Y. Fu
College of Mechanical and Vehicle Engineering, Hunan University,
Changsha 410082, China
E-mail: p_zhang87@hotmail.com
Tel.: +86-731-88822421
Fax: +86-731-88822330

help us deeply understand the deformation and failure of cables, pipelines, optical fibers, as well as DNA molecules [17]. The torsional buckling analysis of a thin circular rod was presented in Ref. [18] by using the famous Kirchhoff–Love model, which neglects the transverse shear and axial extension effects. Thompson and Champneys [17] indicated that the torsional rod would have a helical buckling mode firstly and then encounter a localized writhing in the post-buckling process. After that, a unified framework for identifying these two modes was introduced in Ref. [19] as a following study. For thin elastic rods with noncircular cross-sections, a general model was introduced by Liu and Zu in Ref. [20], where both the deformation and stability problems are discussed.

Compared with cylindrical shells and elastic rods, the stability analyses of coated cylinders are less focused, of which most are for axial compression and external pressure loads, but none for torques, as reviewed in Ref. [2]. On the other hand, researchers usually adopt the Winkler or Pasternak elastic foundation model to represent the compliant core [21] due to their simplicity. However, the equivalent stiffness of these elastic foundation models is quite difficult to be determined, which is related to the core-shell stiffness ratio, thickness ratio as well as different buckling modes. Fortunately, these shortcomings can all be overcome by introducing a three-dimensional elastic core model, as presented in the following text.

Our aim in this paper is to establish a general model for torsional buckling analysis of cylinders with hard coatings. Instead of the approximate elastic foundation models, three-dimensional elasticity theories are used to obtain the deformation of the core, while the coating layer is modeled as a thin shell. It should be noted that the torsional buckling behavior of core-shell structures contains features of both hollow shells and elastic rods, meaning that surface rippling or global helical buckling modes may occur due to the interactions between cores and surface coatings, which needs to be considered carefully in the buckling mode identification process. In addition, the lengths of the cylinders also affect the torsional buckling characteristics, which will be discussed in detail later on.

2 The model

Figure 1 shows the considered elastic circular cylinder with a surface coating layer, which is placed in a cylindrical coordinate system o-$r\theta z$. The thickness and mid-plane radius of the surface layer are denoted as t and R, respectively. As a result, the inner and outer radii can also be deduced as $R_i = R - 0.5t$ and $R_o = R + 0.5t$, respectively. It is assumed that the surface layer is quite thin ($t \ll R$) and harder than the core.

For simplification, the coordinate variables r, θ and z are replaced by 1, 2, and 3, respectively. Then the infinitesimal elastic strain components can be written as

$$\begin{aligned}
\varepsilon_{11} &= u_{1,1}, \\
\varepsilon_{22} &= u_{2,2}/r + u_1/r, \\
\varepsilon_{33} &= u_{3,3}, \\
\varepsilon_{13} &= (u_{1,3} + u_{3,1})/2, \\
\varepsilon_{23} &= (u_{2,3} + u_{3,2}/r)/2, \\
\varepsilon_{12} &= (u_{1,2}/r + u_{2,1} - u_2/r)/2,
\end{aligned} \tag{1}$$

where ε_{ij} and u_i $(i, j = 1, 2, 3)$ are the strain tensor and displacement vector, respectively. The subscript comma represents the derivative respect to the corresponding coordinate variable.

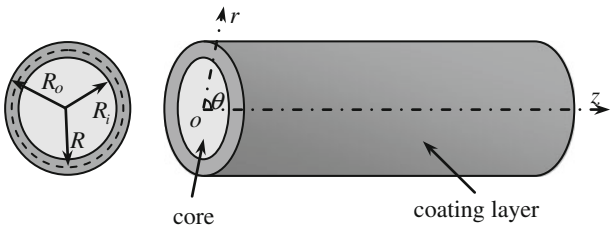

Fig. 1 Sketch of an elastic circular cylinder with a hard coating layer

Linear elastic stress–strain relationship is adopted and that for the core is

$$\sigma_{ij} = 2\mu\left(\varepsilon_{ij} + \frac{\nu}{1-2\nu}\delta_{ij}\,\varepsilon_{mm}\right), \tag{2}$$

where σ_{ij} and δ_{ij} are the stress tensor and Kronecker-delta tensor, respectively. The shear modulus and Poission's ratio of the core are μ and ν. Obviously, the stress–strain relationship for the surface coating layer is similar to Eq. (2), which can be obtained by changing the two material constants as μ_s and ν_s, respectively.

The cylinder is assumed to be straight and perfect initially and allowed to have a uniform residual stress field $\sigma_{22} = \sigma_{33} = \sigma_s$ within the surface layer. These residual stresses may be induced by manufacturing or surface treatment, while for nanowires, there exist intrinsic surface stresses. If the coating layer in Fig. 1 is removed, the cylinder would twist uniformly about its axis when applying a torque at its ends, as introduced in many text books. However, the torsional characteristics would be even more complex for the considered model due to the interactions between the core and surface layer, which may induce the buckling phenomena.

3 Surface rippling deformation analysis

Hollow cylindrical shells usually prefer local buckling modes when twisting. Similarly, this kind of surface rippling mode also plays a dominant role for a coated cylinder. In the following part, we will present analytical solutions for the deformation of a core-shell cylinder.

3.1 Deformation of the core

The deformation of the core must be studied first to obtain the interaction forces of it with the surface layer. Here, we abandon the elastic foundation models mentioned in Section 1 and deduce the unknown displacements by solving Navier's equation [22] for three-dimensional problems, as

$$\begin{aligned}
\Delta u_1 - \frac{2}{r^2}u_{2,2} - \frac{1}{r^2}u_1 + \frac{1}{1-2\nu}\left(u_{1,1} + \frac{1}{r}u_1 + \frac{1}{r}u_{2,2} + u_{3,3}\right)_{,1} &= 0,\\
\Delta u_2 + \frac{2}{r^2}u_{1,2} - \frac{1}{r^2}u_2 + \frac{1}{1-2\nu}\frac{1}{r}\left(u_{1,1} + \frac{1}{r}u_1 + \frac{1}{r}u_{2,2} + u_{3,3}\right)_{,2} &= 0,\\
\Delta u_3 + \frac{1}{1-2\nu}\left(u_{1,1} + \frac{1}{r}u_1 + \frac{1}{r}u_{2,2} + u_{3,3}\right)_{,3} &= 0,
\end{aligned} \tag{3}$$

where Δ is the Laplacian operator, as $\Delta u = u_{,11} + r^{-1}u_{,1} + r^{-2}u_{,22} + u_{,33}$.

The displacement field within the core after surface rippling is assumed to be

$$\begin{pmatrix} u_1 \\ u_2 \\ u_3 \end{pmatrix} = \begin{pmatrix} 0 \\ \phi r z \\ 0 \end{pmatrix} + \begin{pmatrix} U_1(r)\sin[k(\theta - \eta z)] \\ U_2(r)\cos[k(\theta - \eta z)] \\ U_3(r)\cos[k(\theta - \eta z)] \end{pmatrix}, \tag{4}$$

where the first term of the right-hand part indicates the uniform torsional deformation with ϕ the torsional angle per unit length, which is the same with the classical torsion problem for a circular rod. The second term indicates the additional deformation after surface rippling, as illustrated in Fig. 2. k is the wave number in the circumference direction, and η is actually a parameter characterizing the rippling orientation. When η increases from 0 to ∞, the rippling direction moves from perpendicular to parallel to the axial direction. This change can also be observed in Fig. 2, where the $\eta = R^{-1}$ cases have more waves in the axial direction than the $\eta = 1.5R^{-1}$ ones.

Unlike the Cartesian coordinate case [23], it is quite difficult to solve the Navier's equation directly in the cylindrical coordinate system, and a circuitous route must be taken to obtain analytical solutions. To achieve that aim, the Papkovich–Neuber potential Φ_i $(i = 0, 1, 2, 3)$ [22] should be introduced first, as

$$\begin{aligned}
u_1 &= \Phi_1 - a(\Phi_0 + r\Phi_1 + z\Phi_3)_{,1},\\
u_2 &= \Phi_2 - ar^{-1}(\Phi_0 + r\Phi_1 + z\Phi_3)_{,2},\\
u_3 &= \Phi_3 - a(\Phi_0 + r\Phi_1 + z\Phi_3)_{,3},
\end{aligned} \tag{5}$$

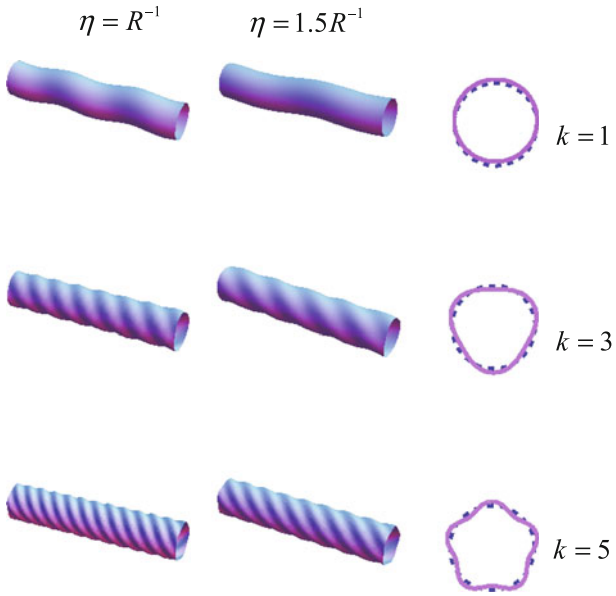

Fig. 2 Surface rippling morphology of an elastic cylinder in torsion for different k and η values. The *rightmost column* illustrates the deformed cross sections (*solid line*) and the undeformed ones (*dash line*)

where $a = 1/[4(1-\nu)]$. It has been demonstrated that Eq. (3) can be satisfied automatically if the displacement potential Φ_i $(i = 0, 1, 2, 3)$ obeys the following equations [22]:

$$\begin{aligned} \Delta\Phi_0 = \Delta\Phi_3 = 0, \\ \Delta\Phi_1 - 2r^{-2}\Phi_{2,2} - r^{-2}\Phi_1 = 0, \\ \Delta\Phi_2 + 2r^{-2}\Phi_{1,2} - r^{-2}\Phi_2 = 0. \end{aligned} \tag{6}$$

Thus, it is assumed that Φ_i $(i = 0, 1, 2, 3)$ have the following form, in accordance with the displacement field of Eq. (4):

$$\begin{aligned} \Phi_0 &= \varphi_0(r)\sin[k(\theta - \eta z)], \\ \Phi_1 &= \varphi_1(r)\sin[k(\theta - \eta z)], \\ \Phi_2 &= \varphi_2(r)\cos[k(\theta - \eta z)] + \phi r z, \\ \Phi_3 &= \varphi_3(r)\cos[k(\theta - \eta z)]. \end{aligned} \tag{7}$$

After substituting Eq. (7) into Eq. (6) and omitting the spatial variables θ and z, the governing equations of $\varphi_i(r)$ $(i = 0, 1, 2, 3)$ are obtained as follows:

$$\begin{aligned} r^2\varphi_{0,11} + r\varphi_{0,1} - (k^2 + k^2\eta^2 r^2)\varphi_0 = 0, \\ r^2\varphi_{1,11} + r\varphi_{1,1} - [(1+k^2) + k^2\eta^2 r^2]\varphi_1 + 2k\varphi_2 = 0, \\ r^2\varphi_{2,11} + r\varphi_{2,1} - [(1+k^2) + k^2\eta^2 r^2]\varphi_2 + 2k\varphi_1 = 0, \\ r^2\varphi_{3,11} + r\varphi_{3,1} - (k^2 + k^2\eta^2 r^2)\varphi_3 = 0. \end{aligned} \tag{8}$$

It is obvious that the middle two equations in Eq. (8) are still difficult to be solved directly, and need to be decoupled by introducing two new functions as

$$\begin{aligned} f(r) = \varphi_1 + \varphi_2, \\ g(r) = \varphi_1 - \varphi_2. \end{aligned} \tag{9}$$

Thus, the governing equations of functions $f(r)$ and $g(r)$ can be readily obtained by substituting Eq. (9) into the middle two equations of Eq. (8) as

$$\begin{aligned} r^2 f_{,11} + r f_{,1} - [(k-1)^2 + k^2\eta^2 r^2]f = 0, \\ r^2 g_{,11} + r g_{,1} - [(k+1)^2 + k^2\eta^2 r^2]g = 0. \end{aligned} \tag{10}$$

The solutions of the first and last equations in Eq. (8) as well as Eq. (10) can be easily obtained by introducing Bessel functions. Finally, the solutions of φ_i are as follows:

$$\begin{aligned}\varphi_0 &= c_0 I_k,\\ \varphi_1 &= c_1 I_{k-1} + c_2 I_{k+1},\\ \varphi_2 &= c_1 I_{k-1} - c_2 I_{k+1},\\ \varphi_3 &= c_3 I_k,\end{aligned} \tag{11}$$

where $I_k \triangleq I_k(k\eta r)$ is the kth order modified Bessel function of the first kind and c_i $(i = 0, 1, 2, 3)$ are unknown coefficient constants. It should be mentioned that the general solutions of φ_i also contain terms of the second kind modified Bessel functions, as K_{k-1}, K_k and K_{k+1}, which have been omitted to avoid the singularity at $r = 0$ point. In addition, it is also found that c_3 must be equal to zero to satisfy the presumed displacement fields, or else the rippling mode would have a linear term of variable z and is not in period, which can be easily verified by substitution of Eq. (11) into Eq. (5). At last, the rippling displacement functions are

$$\begin{aligned}U_1 &= (1-a)(c_1 I_{k-1} + c_2 I_{k+1}) - ak\eta(c_0 I'_k + c_1 r I'_{k-1} + c_2 r I'_{k+1}),\\ U_2 &= c_1(1-ak) I_{k-1} - c_2(1+ak) I_{k+1} - akr^{-1} c_0 I_k,\\ U_3 &= ak\eta(c_0 I_k + c_1 r I_{k-1} + c_2 r I_{k+1}),\end{aligned} \tag{12}$$

where $I'_k \triangleq \partial I_k(k\eta r)/\partial(k\eta r)$. Until now, the displacement field in Eq. (4) is presented analytically with only three unknown constants $c_i (i = 0, 1, 2)$.

The stress field can be readily obtained after substituting the deduced displacement field into Eq. (1) and then to Eq. (2). Here, we only present the stress components in r direction, which interact with the surface layer directly, as

$$\begin{aligned}\sigma_{11} &= \frac{2\mu}{1-2\nu}\left[(1-\nu)U_{1,1} + \nu\left(-\frac{1}{r}kU_2 + \frac{1}{r}U_1\right) + \nu k\eta U_3\right]\sin[k(\theta-\eta z)],\\ \sigma_{12} &= \mu\left(\frac{1}{r}kU_1 + U_{2,1} - \frac{1}{r}U_2\right)\cos[k(\theta-\eta z)],\\ \sigma_{13} &= \mu(-k\eta U_1 + U_{3,1})\cos[k(\theta-\eta z)].\end{aligned} \tag{13}$$

Further, these stresses can be written in the form of c_i by substituting Eq. (12) into Eq. (13), as

$$\begin{aligned}\sigma_{11} &= (S_{11}c_0 + S_{12}c_1 + S_{13}c_2)\sin[k(\theta-\eta z)],\\ \sigma_{12} &= (S_{21}c_0 + S_{22}c_1 + S_{23}c_2)\cos[k(\theta-\eta z)],\\ \sigma_{13} &= (S_{31}c_0 + S_{32}c_1 + S_{33}c_2)\cos[k(\theta-\eta z)],\end{aligned} \tag{14}$$

where the coefficient functions $S_{ij}(i, j = 1, 2, 3)$ are listed in Appendix A as Eq. (A1).

3.2 Deformation of the coating

Instead of complex three-dimensional analyses, the thin shell model is adopted here to study the deformation of the hard surface layer, which is accurate enough for thin coating cases. Thus, the displacement field within the coating is

$$\begin{pmatrix}u_1\\ u_2\\ u_3\end{pmatrix} = \begin{pmatrix}u_1^0\\ \frac{r}{R}u_2^0 - \frac{1}{R}(r-R)u_{1,2}^0\\ \frac{r}{R}u_3^0 - (r-R)u_{1,3}^0\end{pmatrix}, \tag{15}$$

where u_1^0, u_2^0, and u_3^0 are the displacement components at the coating's mid-plane $(r = R)$, as

$$\begin{pmatrix}u_1^0\\ u_2^0\\ u_3^0\end{pmatrix} = \begin{pmatrix}0\\ \phi Rz\\ 0\end{pmatrix} + \begin{pmatrix}U_1^0\sin[k(\theta-\eta z)]\\ U_2^0\cos[k(\theta-\eta z)]\\ U_3^0\cos[k(\theta-\eta z)]\end{pmatrix}. \tag{16}$$

Similar to Eq. (4), the right-hand part of the above equation also contains two terms: one for uniform torsional deformation and the other for additional rippling deformation. It should be noted that this displacement field is not suitable for thick coating cases, which require higher-order shell models or three-dimensional elasticity analyses [12].

Equilibrium equations of the coating layer by taking into account the uniform torsion and residual stress effects are

$$\begin{aligned}
\frac{t}{A}\left[\sigma_s\left(u^0_{1,33}+\frac{1}{R^2}u^0_{1,22}\right)+2\mu_s\phi u^0_{1,23}\right]-\left(\frac{t^2}{12}\Delta_s^2 u^0_1+\frac{\nu_s}{R}u^0_{3,3}+\frac{1}{R^2}u^0_{2,2}+\frac{1}{R^2}u^0_1\right)&=\frac{1}{A}\,\sigma_{11}|_{r=R_i}\,,\\
\frac{1+\nu_s}{2R}u^0_{3,23}+\frac{1-\nu_s}{2}u^0_{2,33}+\frac{1}{R^2}u^0_{2,22}+\frac{1}{R^2}u^0_{1,2}&=\frac{1}{A}\,\sigma_{12}|_{r=R_i}\,,\\
u^0_{3,33}+\frac{1-\nu_s}{2}\frac{1}{R^2}u^0_{3,22}+\frac{1+\nu_s}{2R}u^0_{2,23}+\frac{\nu_s}{R}u^0_{1,3}&=\frac{1}{A}\,\sigma_{13}|_{r=R_i}\,,
\end{aligned}\tag{17}$$

where $A=2\mu_s t/(1-\nu_s)$ and $\Delta_s u=R^{-2}u_{,22}+u_{,33}$. The square bracket term of the first equation in Eq. (17) is the effect of in-plane residual stresses and the applied torques, which is different from the common thin shells [24]. The right-hand terms of Eq. (17) are the interaction forces between the core and the coating layer, which have been given in Eq. (14). It should be mentioned that a negative residual stress field σ_s may induce buckling of the shell before torsion. For instance, a buckling mode of $\phi=\eta=0$ and $k=1$ in Eq. (16) would occur for a hollow shell if $\sigma_s\le -AtR^{-2}/12$. Other buckling modes can also be predicted easily from Eq. (17) and would not be presented in details here.

After substituting the assumed displacements of Eq. (16) into Eq. (17), one obtains the equilibrium equations only with variables U_i^0, as

$$\boldsymbol{T}\cdot\boldsymbol{x}_2=\tilde{\boldsymbol{S}}\cdot\boldsymbol{x}_1,\tag{18}$$

where $\boldsymbol{x}_1=[c_0\ c_1\ c_2]^{\mathrm{T}}$, $\boldsymbol{x}_2=[U_1^0\ U_2^0\ U_3^0]^{\mathrm{T}}$, and $\tilde{\boldsymbol{S}}=\boldsymbol{S}|_{r=R_i}$ is the interfacial value of $\boldsymbol{S}$. The coefficient matrix $\boldsymbol{T}$ is symmetric with components listed in Appendix A as Eq. (A2).

4 Buckling analysis

Either the surface rippling or global buckling mode may occur when the considered cylinder is in torsion. In what follows, methods to obtain the critical torsional angle and identify buckling modes would be introduced. Moreover, effects of the cylinder lengths are also discussed.

4.1 Surface rippling mode

The interactions between the core and surface layer have been taken into account as the right-hand terms of Eq. (17). In addition to that, there are also three displacement continuation conditions at the interface, as

$$\begin{aligned}
r=R_i:\quad & U_1=U_1^0,\\
& U_2=\frac{r}{R}U_2^0-\left(\frac{r}{R}-1\right)kU_1^0,\\
& U_3=\frac{r}{R}U_3^0+(r-R)k\eta U_1^0.
\end{aligned}\tag{19}$$

The above equation can also be written in a matrix form after taking Eq. (12) into it, as

$$\tilde{\boldsymbol{X}}\cdot\boldsymbol{x}_1=\boldsymbol{Y}\cdot\boldsymbol{x}_2,\tag{20}$$

where $\tilde{\boldsymbol{X}}=\boldsymbol{X}|_{r=R_i}$ with $\boldsymbol{X}$ and $\boldsymbol{Y}$ presented in Appendix A as Eq. (A3) and Eq. (A4), respectively.

Equation (18) and Eq. (20) can be rewritten in a combined form as

$$\begin{pmatrix}\tilde{\boldsymbol{S}} & -\boldsymbol{T}\\ \tilde{\boldsymbol{X}} & -\boldsymbol{Y}\end{pmatrix}\cdot\begin{pmatrix}\boldsymbol{x}_1\\ \boldsymbol{x}_2\end{pmatrix}=0.\tag{21}$$

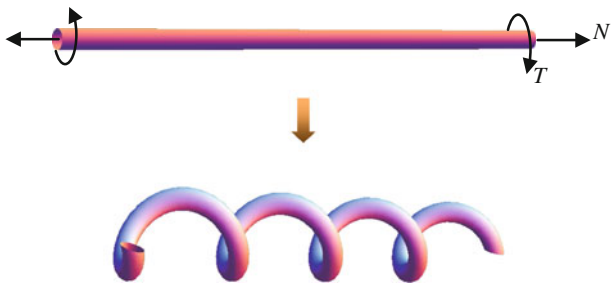

Fig. 3 Global helical buckling mode of an elastic rod under combined loading

Actually, the above equation is the stress and displacement continuation conditions at the interface. This equation only contains six unknown variables, as $c_0, c_1, c_2, U_1^0, U_2^0$, and U_3^0. Then, the torsional angle ϕ can be readily obtained by vanishing of the coefficient matrix's determinant in Eq. (21), as

$$\phi = F(k, \eta), \tag{22}$$

where $F(k, \eta)$ is an explicit formula with variables k and η. The detailed form of F is a little long and will not be presented here, but can easily be deduced through the software *Mathematica*. After that, the critical torsional angle ϕ_c, which indicates the buckling occurrence, can be obtained by searching the minimum ϕ for any possible k and η values, as

$$\phi_c = \min\ F(k, \eta) \qquad \text{for}\ \ \eta > 0\ \&\ \ k = 1, 2, \ldots \infty. \tag{23}$$

It should be mentioned that ϕ is only contained in T_{11} of Eq. (21). Then, if we denote the torsional angle with none residual stress effect as ϕ^0, the torsional angle ϕ can be written in another form as follows:

$$\phi = \phi^0 + \frac{\sigma_s \eta}{2\mu_s}. \tag{24}$$

Note that the above equation does not imply $\phi_c = \phi_c^0 + 0.5\sigma_s\eta/\mu_s$, because ϕ is also related to the wave number k. When different residual stress fields exist, one must look for the critical torsional angle through Eq. (23) from the beginning.

Furthermore, the present model would degrade to a hollow shell if the core's deformation is ignored, and the torsional angle for that case has the simple formula

$$\phi(k, \eta) = \frac{k^2 t^2 (R^{-2} + \eta^2)^2}{12(1 - \nu_s)\eta} + \frac{(1 + \nu_s) R^{-2} \eta^3}{k^2 (R^{-2} + \eta^2)^2} + \frac{\sigma_s k (R^{-2} + \eta^2)}{2\mu_s \eta}. \tag{25}$$

4.2 Global buckling mode

An elastic rod is used to encounter a helical buckling mode in combined torsion and compression, as illustrated in Fig. 3. This buckling characteristic is also applicable to coated cylinders. Here, we only consider the compressive force induced by σ_s. Thus, the torque and axial force for the present model can be written as

$$\begin{aligned} T &= 0.5\pi\phi[(R_o^4 - R_i^4)\mu_s + R_i^4 \mu], \\ N &= 2\pi R t \sigma_s. \end{aligned} \tag{26}$$

The Kirchhoff–Love rod model is adopted here, of which the critical condition for global helical buckling is [17,18]

$$T_c^2 = -4BN_c \tag{27}$$

where $B = 0.5\pi[\mu_s(1+\nu_s)(R_o^4 - R_i^4) + \mu(1+\nu)R_i^4]$ is the bending stiffness of the cylinder. It can be obtained from Eq. (27) that only a negative axial force may induce the helical morphology and the cylinder buckles

only when the applied torque increases to T_c or the axial force decreases to N_c. Thus, when the surface layer's residual stress field is fixed, the critical torsional angle can be readily obtained from Eqs. (26)–(27) as

$$\phi_c = \frac{4\sqrt{-2\pi B R t \sigma_s}}{\pi[(R_o^4 - R_i^4)\mu_s + R_i^4 \mu]}. \tag{28}$$

Along with ϕ_c, the wavelength of the helical mode can also be written as

$$L_c = \frac{2\pi B}{\sqrt{-BN_c}} = \sqrt{\frac{2\pi B}{-Rt\sigma_s}}. \tag{29}$$

To sum up, a coated cylinder would buckle as the surface rippling mode when applying non-negative residual stresses, or else one must consider both modes carefully and find out which one has the smaller critical torsional angle.

4.3 Cylinder length effects

The assumed displacement fields of Eq. (4) and Eq. (16) do not include the effects of cylinder lengths. However, many filled shells and coated rods have finite sizes in engineering applications. For a cylinder of finite length, the morphology functions of Eq. (4) are assumed as [25]

$$\begin{pmatrix} u_1 \\ u_2 \\ u_3 \end{pmatrix} = \begin{pmatrix} 0 \\ \phi r z \\ 0 \end{pmatrix} + \begin{pmatrix} U_1(r)\sin[k\theta - n\pi z/L] \\ U_2(r)\cos[k\theta - n\pi z/L] \\ U_3(r)\cos[k\theta - n\pi z/L] \end{pmatrix}, \tag{30}$$

where n is the axial wave number and L is the length of the cylinder. The displacement field of the coating layer in this case is similar to Eq. (30) and would not be presented again.

From the comparisons between Eq. (4) and Eq. (30), it is found that η is a series of discrete values for finitely long cylinders, as $\eta = n\pi/(kL)$. Thus, the critical torsional angle of Eq. (23) should be changed as follows:

$$\phi_c = \min\ F\left(k, \frac{n\pi}{kL}\right) \qquad \text{for} \quad k, n = 1, 2, \ldots \infty. \tag{31}$$

The above equation indicates that ϕ_c can be obtained by seeking to the minimum of F for any positive integer k and n.

A finite-length cylinder may also encounter the global helical buckling mode [17]. However, the residual stress σ_s usually has lower order of magnitude, which would induce quite large global buckling wave length $L_c (L_c \sim (-\sigma_s)^{-0.5})$, and it is far longer than the cylinder length ($L_c \gg L$). Thus, the global buckling modes are not easy to occur and would not be studied here.

5 Numerical examples

In what follows, we will quantitatively discuss the torsional buckling characteristics of the coated cylinder, for both infinitely and finitely long cases.

Some dimensionless variables are introduced firstly before the presentation of numerical examples, as

$$(\bar{\phi}_c, \bar{\eta}) = (\phi_c, \eta)R, \quad (\bar{t}, \bar{L}_c, \bar{L}) = (t, L_c, L)R^{-1}, \quad \bar{\mu}_s = \mu_s \mu^{-1}, \quad \bar{\sigma}_s = \sigma_s \mu_s^{-1}. \tag{32}$$

Obviously, $\bar{\phi}_c$ is only related to parameters $\bar{t}$, $\bar{\mu}_s$ and $\bar{\sigma}_s$ for an infinitely long cylinder, while also related to $\bar{L}$ for a finitely long one. What's more, the Poission's ratios of the core and coating layer are both set as $\nu = \nu_s = 0.35$ in this section.

Table 1 Torsional rippling behaviors of elastic cylinders with infinite-lengths

$\bar{\mu}_s$	$\bar{t} = 0.08$			$\bar{t} = 0.10$			$\bar{t} = 0.12$		
	$\bar{\phi}_c$	k	$\bar{\eta}$	$\bar{\phi}_c$	k	$\bar{\eta}$	$\bar{\phi}_c$	k	$\bar{\eta}$
3	0.01088	1	0.1013	0.01481	1	0.1165	0.01912	1	0.1303
5	0.01033	1	0.1069	0.01418	1	0.1220	0.01842	1	0.1357
10	0.009849	1	0.1123	0.01364	1	0.1272	0.01783	1	0.1407
15	0.009674	1	0.1145	0.01345	1	0.1293	0.01763	1	0.1426
20	0.009584	1	0.1157	0.01335	1	0.1304	0.01753	1	0.1436
30	0.009492	1	0.1170	0.01325	1	0.1315	0.01742	1	0.1447
40	0.009445	1	0.1177	0.01320	1	0.1321	0.01737	1	0.1453
50	0.009417	1	0.1181	0.01317	1	0.1325	0.01734	1	0.1456
60	0.009398	1	0.1184	0.01315	1	0.1328	0.01732	1	0.1458
70	0.009384	1	0.1186	0.01313	1	0.1330	0.01730	1	0.1460
80	0.009374	1	0.1187	0.01312	1	0.1331	0.01729	1	0.1461
∞	0.009303	1	0.1198	0.01305	1	0.1341	0.01722	1	0.1471

5.1 Cylinders with infinite lengths

Any possible positive $\bar{\eta}$ and positive integer k values should be considered when implementing the optimization procedure of Eq. (23) to obtain the critical torsional angle for the surface rippling mode. Moreover, Eq. (28) should also be noticed because global buckling modes may occur for negative residual stress cases. Finally the smallest critical torsional angle would indicate the actual buckling mode.

Table 1 shows the torsional buckling behaviors of cylinders with no residual stresses. It can be seen that the critical torsional angles vary with different $\bar{t}$ and $\bar{\mu}_s$ values. Note that the compliant core's effect would diminish as $\bar{\mu}_s$ increases, and the considered cylinder would degrade to a hollow shell when $\bar{\mu}_s \to \infty$. The critical torsional angle $\bar{\phi}_c$ decreases when the coating becomes stiffer or thinner, mainly because the reduction in the core's effect or the cylinder's overall stiffness, respectively. There is only one circumference wave number for all these cases, which indicates that the critical state of an infinitely long cylinder only occurs for $k = 1$ when no residual stress exists. What's more, the rippling orientation parameter $\bar{\eta}$ becomes smaller when the coating layer is softer and thinner. One must seek for a new value of $\bar{\eta}$ to obtain the critical state when the coating's stiffness or thickness changes.

Effects of the residual stress $\bar{\sigma}_s$ on buckling characteristics are also studied, as shown in Fig. 4. For surface rippling modes, the critical torsional angle $\bar{\phi}_c$ decreases when $\bar{\mu}_s$ becomes larger, which is similar to the cases with no residual stresses. However, for the global buckling case, $\bar{\phi}_c$ would become larger with increasing $\bar{\mu}_s$ due to the increase of the cylinder's bending stiffness. When dealing with the torsional buckling problems with negative residual stresses, one must compare the critical torsional angles of these two modes and choose a smaller one. It can be seen in Fig. 4 that the global buckling mode only occurs for quite small $\bar{\sigma}_s$, which is because the surface layer considered here is still very thin ($\bar{t} \leq 0.1$). For a cylinder with thick surface layer or stiff core, the global buckling mode's role would be more significant. In addition, the cylinder is even more stable when $\bar{\sigma}_s$ increases and $\bar{\phi}_c$ and $\bar{\eta}$ become larger correspondingly. Another problem which should be paid attention to in Fig. 4b is that $\bar{\phi}_c \approx 0$ near the point $\bar{\sigma}_s = -2.5 \times 10^{-4}$. This phenomenon occurs because the coated cylinder would buckle as a $k = 1$ and $\bar{\eta} = 0$ mode prior to the torque is applied, as mentioned in Section 3. The critical residual stress predicted for a hollow shell is $\bar{\sigma}_{sc} = -2.3 \times 10^{-4}$, which shows good agreement with the data plotted here. When the surface layer is quite stiff, e.g., $\bar{\mu}_s = \infty$, higher-order surface rippling modes may occur due to the positive surface layer residual stress. This phenomenon is similar to the torsional buckling of an inflated shell, which must be considered carefully when obtaining the critical torsional angle.

5.2 Cylinders with finite lengths

In this section, we will discuss the length's effect on the torsional buckling characteristics of coated cylinders. Cylinders with different lengths and surface layer residual stresses are considered. Taking a cylinder with $\bar{t} = 0.05$, $\bar{\mu}_s = 5$ and $\bar{\sigma}_s = -0.001$ as an example, the global buckling wave length $\bar{L}_c$ is 319, far longer than the cylinder length. Thus, only surface rippling modes are studied for finitely long cylinders.

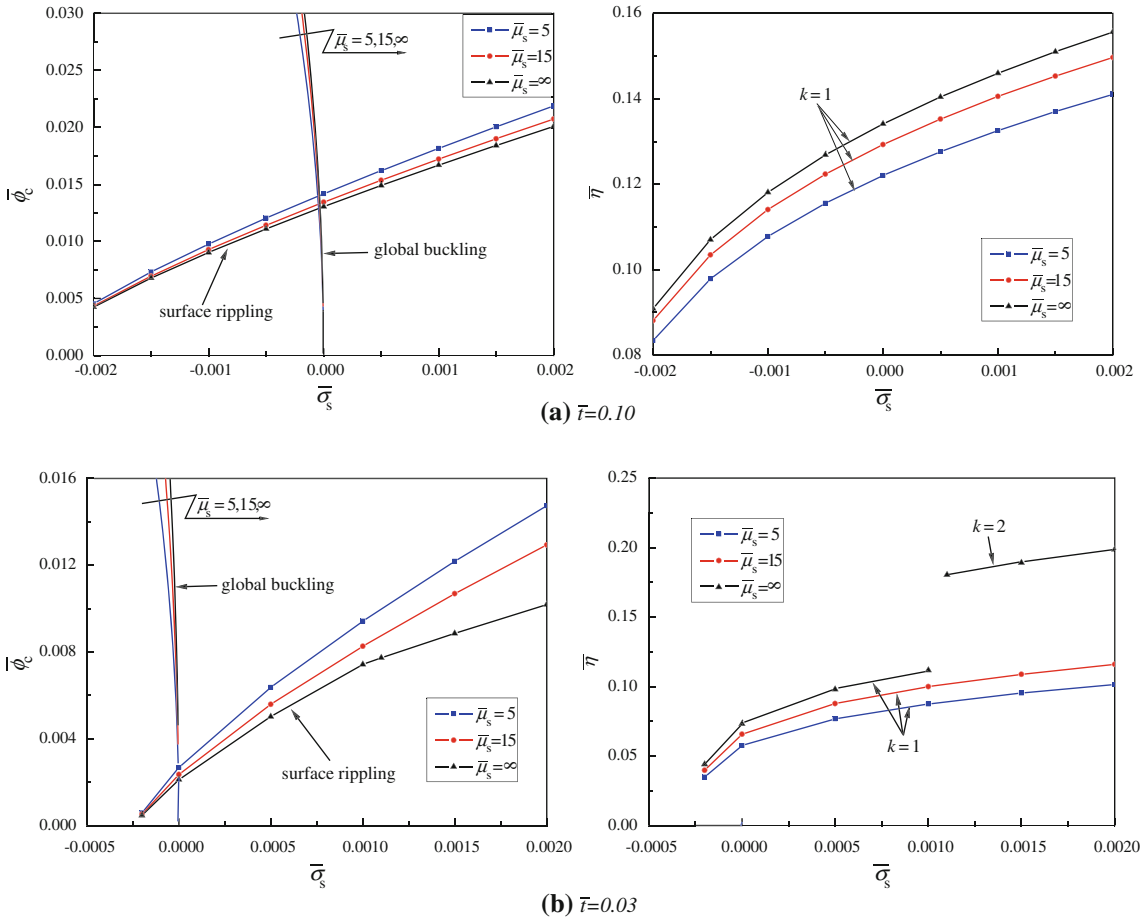

Fig. 4 Effects of the surface layer's residual stresses on the buckling characteristics of coated cylinders

Figure 5 shows the lengths' effect on the critical torsional angles of coated cylinders. The two numbers in the bracket denote the wave numbers (k, n) at the adjacent points. For the cases $\bar{\mu}_s = 5$ and $\bar{\mu}_s = 15$, it is found that only first-order modes occur as $k = n = 1$, and $\bar{\phi}_c$ decreases first and then increases when the cylinder becomes longer. However, if the surface layer is stiff enough, e.g., $\bar{\mu}_s = \infty$, higher-order modes would occur. In addition, the mode with $k = 2$ also occurs for non-residual stress cases when the cylinder is short ($\bar{L} \sim 15$), which is different from the infinitely long cases. With the increase of $\bar{L}$, the circumferential wave number k decreases, while the axial wave number n becomes larger for each order of k. It is also found that the critical torsional angles for finite-length cylinders are always larger than the infinite-length ones. For instance, $\bar{\phi}_c$ is equal to 0.0049 for an infinite-length rod with $\bar{t} = 0.05$, $\bar{\mu}_s = 15$, and $\bar{\sigma}_s = 0$, which coincides with the minimum in Fig. 5a. Similar to the infinite-length case, positive surface layer residual stresses enhance a cylinder's stability, but may change the buckling modes, which should be considered carefully.

At last, the torsional buckling characteristics of a cylinder with different coating thicknesses are studied. As illustrated in Fig. 6a, the critical torsional angle increases when $\bar{\mu}_s$ decreases, and higher-order rippling modes may occur when $\bar{\mu}_s \to \infty$. The circumferential wave number k decreases when the surface layer becomes thicker, while the axial wave number n increases for each order of k. Figure 6b shows the effects of the surface layer residual stresses on the buckling properties of these cases. Note that only the value changes of the critical torsional angle induced by residual stresses are plotted. It is astonishing that the changes are constants for cases without the rippling mode transformation, i.e., k and n are still the same after applying the residual stress. This phenomenon occurs because $\bar{\phi}_c - \bar{\phi}_c^0 = 0.5\bar{\sigma}_s\bar{\eta}$ if k and n are fixed, which can be readily obtained from Eq. (24).

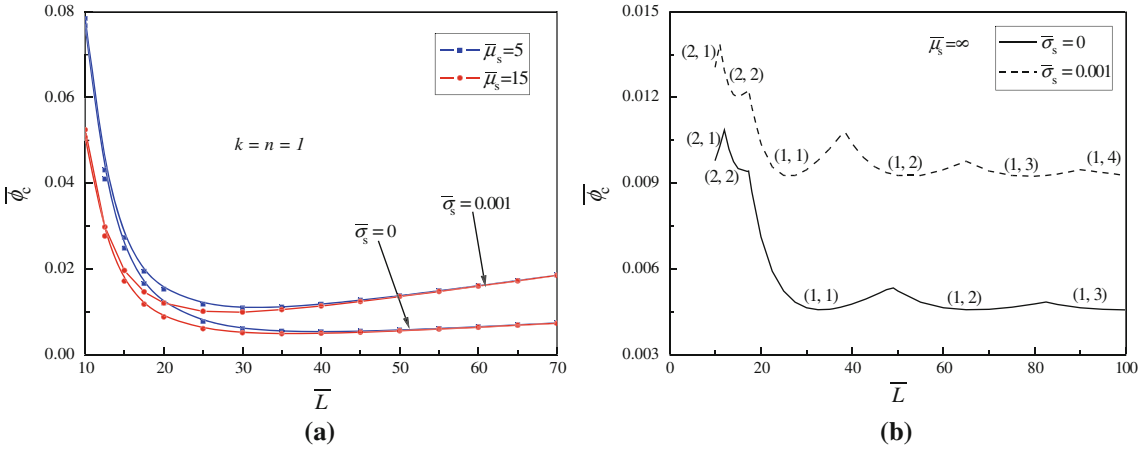

Fig. 5 Critical torsional angles of coated cylinders with finite-lengths ($\bar{t} = 0.05$)

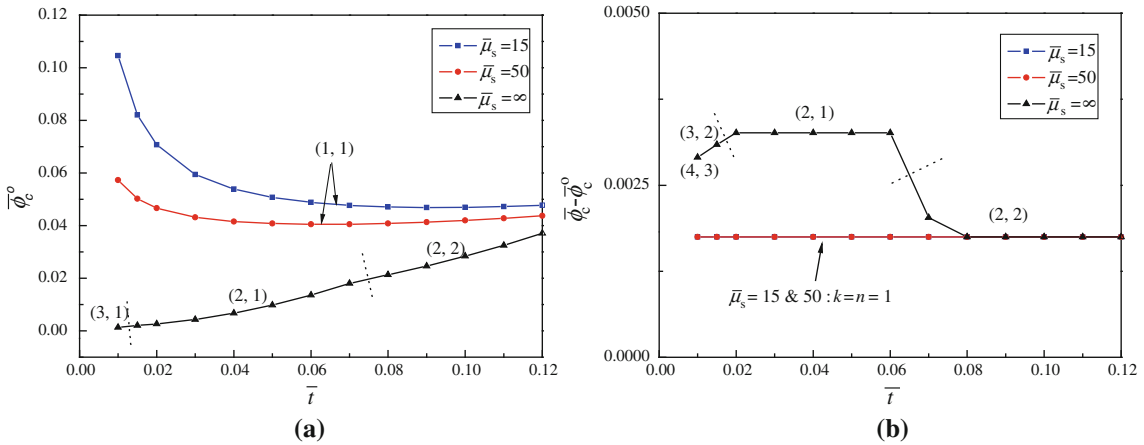

Fig. 6 Effects of the surface layer's thickness on the buckling characteristics of a cylinder with finite-length ($\bar{L} = 10$). $\bar{\phi}_c^o$ and $\bar{\phi}_c$ indicate critical torsional angles of cylinders with the residual stress $\bar{\sigma}_s = 0$ and $\bar{\sigma}_s = 0.001$, respectively

6 Conclusion remarks

In summary, the torsional buckling characteristics of an elastic cylinder with a hard surface layer are studied in this paper. The deformation of the core is obtained analytically from the Navier's equation, and the surface layer is modeled as a thin shell. Both of the surface rippling and global buckling modes are considered for cylinders with either infinite or finite lengths. It is found that the critical torsional angle increases when the surface layer becomes stiffer or thinner. Positive surface layer residual stresses make the rod more stable and sometimes higher-order surface rippling modes may occur. On the contrary, negative residual stress within the surface layer may induce global buckling modes and should be considered carefully. If there exists no surface layer residual stress, an infinite-length cylinder always buckles as the first-order rippling mode, while higher-order rippling modes may occur for a finitely long cylinder with shorter length or stiffer and thinner coating.

The buckling behavior of a coated cylinder is more complicated than for a hollow shell or a homogeneous rod due to the interactions at interfaces. One can also imagine that a complex hierarchical morphology may occur in the post-buckling process: a global buckling mode accompanied with a surface rippling mode. Then the helical or writhe modes would be even more complex but quite interesting, which will be directed toward in our next study.

Acknowledgments We acknowledge support from the National Natural Science Foundation of China through Grant No. 11072076.

Appendix A

The components of $\boldsymbol{S}$ are

$$\begin{aligned}
S_{11} &= 2\mu(1-2\nu)^{-1}\left[(\nu-1)ak\eta I_k'' - ak\eta\nu r^{-1}I_k' + ak^2\nu(r^{-2}+\eta^2)I_k\right],\\
S_{12} &= 2\mu(1-2\nu)^{-1}\{(\nu-1)ak^2\eta^2 r I_{k-1}'' + (1-\nu-2a+a\nu)k\eta I_{k-1}',\\
&\quad + [(1-a-k+ak^2)r^{-1} + ak^2\eta^2 r]\nu I_{k-1}\},\\
S_{13} &= 2\mu(1-2\nu)^{-1}\{(\nu-1)ak^2\eta^2 r I_{k+1}'' + (1-\nu-2a+a\nu)k\eta I_{k+1}',\\
&\quad + [(1-a+k+ak^2)r^{-1} + ak^2\eta^2 r]\nu I_{k+1}\},\\
S_{21} &= 2\mu akr^{-1}(r^{-1}I_k - k\eta I_k'),\\
S_{22} &= \mu[(k-1)r^{-1}I_{k-1} + (1-2ak)k\eta I_{k-1}'],\\
S_{23} &= \mu[(k+1)r^{-1}I_{k+1} - (1+2ak)k\eta I_{k+1}'],\\
S_{31} &= 2\mu ak^2\eta^2 I_k',\\
S_{32} &= \mu[(2a-1)k\eta I_{k-1} + 2ak^2\eta^2 r I_{k-1}'],\\
S_{33} &= \mu[(2a-1)k\eta I_{k+1} + 2ak^2\eta^2 r I_{k+1}'].
\end{aligned} \tag{A1}$$

The components of $\boldsymbol{T}$ are

$$\begin{aligned}
T_{11} &= A^{-1}k^2 t[2\mu_s\phi\eta - \sigma_s(R^{-2}+\eta^2)] - k^4t^2(R^{-2}+\eta^2)^2/12 - R^{-2},\\
T_{12} &= kR^{-2},\\
T_{13} &= -k\eta R^{-1}\nu_s,\\
T_{22} &= -k^2[R^{-2} + (1-\nu_s)\eta^2/2],\\
T_{23} &= (1+\nu_s)R^{-1}k^2\eta/2,\\
T_{33} &= -k^2[\eta^2 + R^{-2}(1-\nu_s)/2].
\end{aligned} \tag{A2}$$

The detailed form of $\boldsymbol{X}$ is

$$\boldsymbol{X} = \begin{pmatrix} -ak\eta I_k' & (1-a)I_{k-1} - rak\eta I_{k-1}' & (1-a)I_{k+1} - rak\eta I_{k+1}' \\ -akr^{-1}I_k & (1-ak)I_{k-1} & -(1+ak)I_{k+1} \\ ak\eta I_k & ak\eta r I_{k-1} & ak\eta r I_{k+1} \end{pmatrix}. \tag{A3}$$

The detailed form of $\boldsymbol{Y}$ is

$$\boldsymbol{Y} = \begin{pmatrix} 1 & 0 & 0 \\ (1-R_i/R)k & R_i/R & 0 \\ (R_i-R)k\eta & 0 & R_i/R \end{pmatrix}. \tag{A4}$$

References

1. Niklas, K.J.: Plant Biomechanics: An Engineering Approach to Plant Form and Function. University of Chicago Press, IL (1992)
2. Karam, G.N., Gibson, L.J.: Elastic buckling of cylindrical shells with elastic cores-I. Anal. Int. J. Solids Struct. **32**, 1259–1283 (1995)
3. Genzer, J., Groenewold, J.: Soft matter with hard skin: From skin wrinkles to templating and material characterization. Soft Matter. **2**, 310–323 (2006)
4. Sepeur, S., Kunze, N., Werner, B., Schmidt, H.: UV curable hard coatings on plastics. Thin Solid Films **351**, 216–219 (1999)
5. Befahy, S. et al.: Thickness and elastic modulus of plasma treated PDMS silica-like surface layer. Langmuir **26**, 3372–3375 (2010)
6. Sun, Z. et al.: Compound core-shell polymer nanofibers by co-electrospinning. Adv. Mater. **15**, 1929–1932 (2003)
7. Wang, L., Pai, C.L., Boyce, M.C., Rutledge, G.C.: Wrinkled surface topographies of electrospun polymer fibers. Appl. Phys. Lett. **94**, 151916 (2009)
8. Wang, G.F., Feng, X.Q.: Surface effects on buckling of nanowires under uniaxial compression. Appl. Phys. Lett. **94**, 141913 (2009)

9. Zhou, L.G., Huang, H.: Are surfaces elastically softer or stiffer? Appl. Phys. Lett. **84**, 1940–1942 (2004)
10. Donnell, L.H.: Stability of thin-walled tubes under torsion. NACA-R-479 (1933)
11. Yamaki, N.: Elastic Stability of Circular Cylindrical Shells.1940–1942 Elsevier, North-Holland (1984)
12. Kim, Y.S., Kardomateas, G.A., Zureick, A.: Buckling of thick orthotropic cylindrical shells under torsion. J. Appl. Mech. **66**, 41–50 (1999)
13. Zhang, X.Q., Han, Q.: Buckling and postbuckling behaviors of imperfect cylindrical shells subjected to torsion. Thin-Walled Struct. **45**, 1035–1043 (2007)
14. Schneider, W., Ribakov, Y.: Collapse analysis of thin walled cylindrical steel shells subjected to constant shear stress. Comput. Struct. **82**, 2463–2470 (2004)
15. Mao, R., Lu, C.H.: Buckling analysis of a laminated cylindrical shell under torsion subjected to mixed boundary conditions. Int. J. Solids Struct. **36**, 3821–3835 (1999)
16. Shen, H.S.: Torsional buckling and postbuckling of FGM cylindrical shells in thermal environments. Int. J. Nonl. Mech. **44**, 644–657 (2009)
17. Thompson, J.M.T., Champneys, A.R.: From helix to localized writhing in the torsional post-buckling of elastic rods. Proc. R. Soc. Lond. A **452**, 117–138 (1996)
18. Love, A.E.H.: A Treatise on the Mathematical Theory of Elasticity, 4th edn. Dover Publications, New York (1944)
19. Van Der Heijden, G.H.M., Thompson, J.M.T.: Helical and localized buckling in twisted rods: a unified analysis of the symmetric case. Nonl. Dyn. **21**, 71–99 (2000)
20. Liu, Y.Z., Zu, J.W.: Stability and bifurcation of helical equilibrium of a thin elastic rod. Acta Mech. **167**, 29–39 (2004)
21. Myint-U, D.T.: Post buckling behavior of axially compressed core-filled cylinders **49**:423–426 (2006)
22. Sadd, M.H.: Elasticity: Theory, Applications, and Numerics. Elsevier, Butterworth-Heinemann (2005)
23. Li, B., Huang, S.Q., Feng, X.Q.: Buckling and postbuckling of a compressed thin film bonded on a soft elastic layer: a three-dimensional analysis. Arch. Appl. Mech. **80**, 175–188 (2010)
24. Gol' denveizer, A.L.: Theory of Elastic Thin Shells. Pergamon Press, New York (1961)
25. Lu, Y.J., Wang, X.: Combined torsional buckling of multi-walled carbon nanotubes. J. Phys. D Appl. Phys. **39**, 3380–3387 (2006)